# Anomalous transport in Charney-Hasegawa-Mima flows

Xavier Leoncini, Olivier Agullo, Sadruddin Benkadda, George M. Zaslavsky

# Anomalous transport in Charney-Hasegawa-Mima flows

Xavier Leoncini,* Olivier Agullo, and Sadruddin Benkadda
*PIIM, Université, de Provence, CNRS, Centre Universitaire de Saint Jerome, F-13397 Marseilles, France*

George M. Zaslavsky†
*Courant Institute of Mathematical Sciences, New York University, 251 Mercer Street, New York, New York 10012, USA*
*and Department of Physics, New York University, 2-4 Washington Place, New York, New York 10003, USA*
(Received 1 December 2004; revised manuscript received 26 April 2005; published 24 August 2005)

The transport properties of particles evolving in a system governed by the Charney-Hasegawa-Mima equation are investigated. Transport is found to be anomalous with a nonlinear evolution of the second moments with time. The origin of this anomaly is traced back to the presence of chaotic jets within the flow. All characteristic transport exponents have a similar value around $\mu=1.75$, which is also the one found for simple point vortex flows in the literature, indicating some kind of universality. Moreover, the law $\gamma=\mu+1$ linking the trapping-time exponent within jets to the transport exponent is confirmed, and an accumulation toward zero of the spectrum of the finite-time Lyapunov exponent is observed. The localization of a jet is performed, and its structure is analyzed. It is clearly shown that despite a regular coarse-grained picture of the jet, the motion within the jet appears as chaotic, but that chaos is bounded on successive small scales.

DOI: 10.1103/PhysRevE.72.026218 PACS number(s): 05.45.Ac, 05.45.Pq, 47.27.Pa, 52.25.Fi

## I. INTRODUCTION

Understanding transport in turbulent magnetized plasma is a task of fundamental importance. In these plasma, transport problems are often related to confinement, which is one of the issues confronting the realization of magnetically confined controlled fusion devices. As the literature evolves, there has been more and more evidence showing that the transport properties can be anomalous, in the sense that transport may not be correctly described by Gaussian kinetics, but by what is now called "strange kinetics" [1]. In this regard, transport phenomena in turbulent magnetized plasma are part of the ever-growing number of physical systems displaying anomalous properties [2–5]. A full understanding of these phenomena is far from being complete, and in many regards, a full-blown theory able to capture and describe correctly these "strange kinetics" has not yet appeared. There seems, nevertheless, to be a common agreement to link these phenomena to Levy-type processes and their generalizations. Moreover, the use of fractional derivatives in Fokker-Plank-Kolmogorov-type equations captures qualitatively some of the transport properties and is thus a good step toward a proper description of anomalous transport [6].

The link between the Hamiltonian dynamics and the kinetics at the origin of anomalous transport properties are relatively well understood when dealing with low-dimensional systems, such as a time periodic flow, that belong to the class of $1\frac{1}{2}$ degrees of freedom Hamiltonians. The dynamics in these systems is not ergodic—a well-defined stochastic sea, with chaotic dynamics, filled with various islands of quasiperiodic dynamics composes the phase space. The anomalous properties and their multifractal nature are then linked to the existence of islands within the stochastic sea and the phenomenon of stickiness observed around them [7,8]. However, when dealing with more complex systems, the loss of time periodicity complicates the picture. For instance, in geophysical flows or two-dimensional (2D) plasma turbulence, the islands that were static and well localized in phase space are replaced by "coherent structures," which have a life of their own. Hence, tackling the origin of anomalous transports from the chaotic dynamics of individual tracers becomes more subtle. Recently, the existence of a hidden order for the tracers that exhibits their possibility to travel in each other's vicinity for relatively large times was exhibited [9]. This order is related to the presence within the system of chaotic jets [10,11]. These chaotic jets can be understood as moving clusters of particles within a specific domain for which the motion appears as almost regular from a coarse-grained perspective. Typically, the chaotic motion of the tracers is confined within the characteristic scale of a given jet, within which nearby tracers are trapped. From another point of view, looking for chaotic jets can be understood as a particular case of measurements of space-time complexity [12].

The purpose of this paper is to study transport properties and to look for chaotic jets in a model of two-dimensional turbulence that applies either in the plasma context, where it is known as the Hasegawa-Mima equation [13], or in the geophysical one, where one speaks about the Charney equation (see, for instance, [14]). In this setting, Annibaldi *et al.* have already shown strong evidence of anomalous transport of passive particles [3,15]; hence, the search for chaotic jets is expected to give some clues about the origin of anomalous transport in these systems—for instance, to identify the structures responsible for such transport. Indeed, in [9], it was clearly shown that trapping within chaotic jets resulted in anomalous transport. Moreover, it appeared that jets were localized around the coherent structures of systems, namely, the vortex cores, and that the structure of the jets was itself a hierarchy of jets within jets, reminiscent of the multifractal

*Electronic address: Xavier.Leoncini@up.univ-mrs.fr
†Electronic address: zaslav@cims.nyu.edu

 

nature of transport observed in $1\frac{1}{2}$ degrees of freedom Hamiltonian systems [8]. Hence, the goal of this paper may be seen as twofold. First, we want to understand the origin of anomalous transport in a model of two-dimensional plasma turbulence. And second, since we are using chaotic jets to track this origin, we are at the same time testing the existence of these jets in a more complex setting than the system of point vortices used in [9]. Once the presence of jets is confirmed, we may be able to speculate that the different anomalous transport behaviors portrayed in references such as [2,16–20] may all find their origin in the presence of long-lived chaotic jets in the considered systems.

The paper is organized as follows: In Sec. II, the basic definitions are introduced. A brief introduction to the Charney-Hasegawa-Mima equation is given. Then, the dynamics of test particles is given, and the Lagrangian approach to transport in this setting is discussed. In Sec. III, the dynamical evolution of the field and of passive test particles, as well as transport properties, are computed numerically. First, the numerical setting is discussed. Then, three regimes corresponding to different parameters for the field evolution are considered. In Sec. IV, we track the origin of anomalous transport in the three, cases considered. First, we recall the definition of a chaotic jet and present the numerical method used to detect these jets. We then present the statistical results related to trapping time within jets and analyze the origin of anomalous transport by localizing the jets and by describing their structure. In Sec. V, we present our conclusions.

## II. BASIC DEFINITIONS

### A. The Charney-Hasegawa-Mima equation

The Charney-Hasegawa-Mima equation can be written in the following form:

$$\partial_t \Omega + [\Omega, \Phi] = 0, \tag{1}$$

$$\Omega = \Phi - \lambda \Delta \Phi + gx, \tag{2}$$

where $[\cdot\,,\cdot]$ corresponds to the Poisson brackets, $\Omega$ is a generalized vorticity given by Eq. (2), $\Phi$ is a potential, and $\lambda$ and $g$ are parameters.

Typically, Eqs. (1) and (2) can either describe the evolution of an anisotropic plasma, and are then referred to as the Hasegawa-Mima equation, or the evolution of geostrophic flows, in which context they are known as the Charney equation. This formal identity has an advantage, as the results obtained in this paper for transport properties should apply in either context.

It is, however, important to be able to put the results back in a physical context. With this in mind, we provide in the next section a short derivation of Eqs. (1) and (2) in both the anisotropic plasma configuration and the geostrophic approximation.

### B. Wave-vortex paradigm equation for two-dimensional flows

#### *1. The Hasegawa-Mima equation*

We begin by considering a magnetized anisotropic plasma, e.g., a plasma with a uniform magnetic field along a direction, $\mathbf{B}=B\mathbf{z}$. We shall also assume that electron response to the turbulent fluctuations of the electric potential $\phi$ is adiabatic, and $n_e(x,y,t)=n_0(x,y)e^{e\phi(x,y,t)/T_e}$, where $n_e$ is the electron density, $n_0$ is the equilibrium plasma density, and $T_e$ is the electron temperature. In the anisotropic plasma, let the cyclotron frequency be $\omega_c=eB/m_i$, and let the hybrid sound speed be $c_s=\sqrt{T_e/m_i}$, where $m_i$ is the ion's mass.

We now consider the motion of cold ions (the ion temperature is assumed to be zero, $T_i=0$) on characteristic time and length scales much larger, respectively, than $1/\omega_c$ and the Debye length $\lambda_D$. In this situation, the plasma is quasineutral $n_i \sim n_e$, and a linear combination of the ion continuity equation and momentum equations gives (see [21] for details)

$$-\boldsymbol{\nabla}\cdot\mathbf{v}_\perp = \frac{D}{Dt}\left(\frac{e\phi}{T_e}\right) + \mathbf{v}_\perp\cdot\boldsymbol{\nabla}\ln n_0 = \frac{1}{\omega+\omega_c}\frac{D}{Dt}(\omega+\omega_c), \tag{3}$$

where $\mathbf{v}_\perp$ is the speed in the plane perpendicular to the magnetic field, and $\omega=\boldsymbol{\nabla}\times\mathbf{v}_\perp$ is the vorticity of the 2D flow. The slow motion of the ions necessarily implies that $\mathbf{v}_\perp \sim \mathbf{v}_D = B_0^{-2}\mathbf{B}_0\times\boldsymbol{\nabla}\phi$, and using the notation $\varphi \equiv e\phi/T_e$, subtraction of the right-hand side terms in (3) readily gives

$$\frac{D}{Dt}(\Delta\varphi - \varphi/l_L^2) - \mathbf{v}_D\cdot\boldsymbol{\nabla}\ln n_0 = 0, \tag{4}$$

where $l_L=c_s/\omega_c$ is the hybrid Larmor radius.

When the plasma is homogeneous ($n_0$=const), the turbulent dynamics of (4) is characterized by the absence of waves and the formation of large vortices. Moreover, in the $l_L\to+\infty$ limit, Eq. (4) becomes formally equivalent to the 2D momentum Euler equation ($\varphi$ being the stream function in the Euler case).

In plasma devices, density is larger in the core than at the boundaries. In this setting, we can often write $n_0(x,y) \sim n_0 e^{-x/L_n}$, where $L_n$ is a characteristic density-gradient length. Using this last approximation, we finally obtain the Hasegawa-Mima equation

$$\frac{D}{Dt}(\Delta\varphi - \varphi/l_L^2) - g\frac{\partial\varphi}{\partial y} = 0, \tag{5}$$

where $g=\omega_c/L_n$.

The inhomogeneous character of the equilibrium density profile in Eq. (5) implies the existence of so-called drift waves in the flow. In particular, the waves deform and interact with the self-organized vortexlike or multipolelike structures and play a key role in their interactions. For instance, the collision of two dipoles can lead to two monopoles plus one dipole plus some radiation [22].

#### *2. The Charney equation*

We now explain the physical nature of the intrinsic length in atmospheric motions. In the context of shallow-water approximation, where the density $\rho$ is uniform, the modeling of the evolution of the atmospheric winds leads to a dynamic equation similar to (3) or (5). Indeed, the atmosphere is characterized by small Ekman and Rossby numbers [14] so that

the motion of the thin incompressible fluid rotating layer (thin with respect to the characteristic scale $L_\perp$ of the horizontal motion) is such that friction forces are very weak compared to the inertial Coriolis force and that pressure forces are balanced by gravity in the vertical direction $\mathbf{z}$ (hydrostatic approximation). As a consequence, the horizontal pressure gradient is independent of the vertical component $z$. It is also proportional to the layer width $h(x,y,t)$ [because of the free boundary condition $p(x,y,h)=p_0=\text{const}$]. It is therefore reasonable to assume that the horizontal velocity field $\mathbf{v}_\perp$ is also $z$ independent, $\mathbf{v}=\mathbf{v}_\perp(x,y,t)+w(x,y,z,t)\mathbf{z}$.

If we assume that the rigid earth surface is locally flat, i.e, $w(z=0)=0$, integration of the incompressibility condition leads to $w=-z\boldsymbol{\nabla}.\mathbf{v}_\perp$ and, in particular, $dh/dt=-h\boldsymbol{\nabla}\cdot\mathbf{v}_\perp$. Moreover, since the forces acting on the fluid are the Coriolis and pressure forces, $\rho f\mathbf{v}_\perp\times\mathbf{z}$ and $-\rho\boldsymbol{\nabla}p$, it is straightforward to deduce from the momentum equation the exact identity $d(\omega+f)/dt=(\omega+f)\boldsymbol{\nabla}\cdot\mathbf{v}_\perp$. It follows that

$$-\boldsymbol{\nabla}\cdot\mathbf{v}_\perp=\frac{D}{Dt}\left(\frac{h}{H_0}\right)=\frac{1}{\omega+f}\frac{D}{Dt}(\omega+f), \tag{6}$$

where we set $h\equiv h+H_0$, with $H_0$ being the mean width of the layer and $h$ the fluctuations around the mean ($h\ll H_0$ by hypothesis). The Coriolis term $f\mathbf{z}$ is the local component of the planetary vorticity $\omega_{planet}$ in the vertical direction, the northward local component $f_n\mathbf{y}$ being negligible. Indeed, the Coriolis force in the horizontal direction is $(-2\rho\omega_{planet}\times\mathbf{v})_\perp=\rho\mathbf{v}_\perp\times f\mathbf{z}+\rho w\mathbf{z}\times f_n\mathbf{y}\sim\rho\mathbf{v}_\perp\times f\mathbf{z}$ because, in the shallow-water approximation, $w/v_\perp=O(H_0/L_\perp)\ll 1$, and far from the equator latitudes, $f_n\sim f$.

It is clear from Eqs. (3) and (6) that in the special limits where the plasma is homogeneous ($n_0=$const.) and the Coriolis parameter $f=f_0$ is taken as constant, both physical systems are formally equivalent. We just have to identify $e\phi/T_e$ with $h/H_0$ and choose as length and time units $(l_L,1/\omega_c)$ or $(l_R,1/f_0)$, where $l_R=\sqrt{gH_0}/f_0$ is the so-called Rossby length. But the similarity holds even for the case of a layer with a slow dynamics ($\omega\ll f$) by taking into account the slow variation of the Coriolis parameter in the northward $y$ direction, $f=f_0+\beta y$, with $\delta f/f_0\ll 1$ ($\beta$-plane approximation). In fact, since the Rossby number is small, we can also make the approximation $\mathbf{v}_\perp\sim\mathbf{v}_D=gf^{-1}\mathbf{z}\times\boldsymbol{\nabla}h$. And by subtracting the right-hand side (r.h.s) terms of (6), we obtain the so-called Charney equation

$$\frac{D}{Dt}(\Delta h-h/l_R^2)-\beta\frac{\partial h}{\partial y}=0. \tag{7}$$

It is clear that (5) and (7) are formally equivalent. However, in the atmospheric case, waves are not generated by a density inhomogeneity but by the earth's rotation. As mentioned earlier, both (5) and (7) can be written in the compact form given by (1), where (2) actually produces $\Omega=\varphi-l_L^2\Delta\varphi-x/L_n$ (the transformations $\varphi\hookrightarrow h$, $g\hookrightarrow\beta$, and $l_L\hookrightarrow l_R$ lead to the Charney equation).

### C. Advection equation

For an incompressible fluid, the evolution of a passive particle is given by the advection equation

$$\dot{z}=v(z,t), \tag{8}$$

where $z(t)$ represents the position of the tracer at time $t$ in the complex plane, and $v(z,t)$ is the velocity field. An important feature of this evolution of passive particles is that the evolution equation given by Eq. (8) can be rewritten as

$$\dot{z}=-i\frac{\partial\Phi}{\partial\bar{z}},\quad \dot{\bar{z}}=i\frac{\partial\Phi}{\partial z}, \tag{9}$$

where the potential $\Phi$ acts as a time-dependent Hamiltonian, and $^-$ denotes the complex conjugate. This Hamiltonian structure is fundamental, as it imposes some constraints on the dynamics of passive tracers, which should be taken into account when carrying a numerical simulation.

### D. Numerical settings

#### 1. Charney-Hasegawa-Mima

Simulations of the Charney-Hasegawa-Mima equation are performed for different initial conditions and choices of parameters. The choices are made to be consistent with the literature, namely, the conditions chosen in [3,15]. The simulations are performed within a square box of size $L=20$ and periodic boundary conditions using a pseudospectral code. In order to compute the evolution of passive tracers accurately, we settled for a somewhat low resolution mesh of $128^2$. Fourier transforms are computed using a fast Fourier algorithm. For the time evolution, we chose a fourth-order Runge-Kunta integration scheme with typical time step $\delta t=0.05$.

In order to avoid numerical instability, as well as a trivial asymptotic behavior, Eq. (1) could not be kept as it is, and a dissipation term $D$ as well as a forcing term $F$ were added

$$\partial_t\Omega+[\Omega,\Phi]=D+F. \tag{10}$$

One can also argue that the dissipation term may be relevant to describe some physical phenomena.

For the dissipation, we used a hyperviscous term $D=\nu(\nabla\Omega)^4$. For the forcing, we used a term whose Fourier transform is

$$\hat{F}(k_x,k_y)=F_0\frac{1}{\sqrt{\nu\sum_k k^4}}e^{i\varphi(k_x,k_y)}, \tag{11}$$

where for any $(k_x,k_y)$, $\varphi(k_x,k_y)$ is a random phase uniformly distributed on the circle, and $k$ runs over an interval centered on $k_0$ with a range $\delta k$. One can set also a time dependency by regularly updating the realization of the random phases.

The initial condition is given by the following choice for the $\Omega'=\Phi-\lambda\Delta\Phi$ field:

$$\Omega'=A_0\sum\frac{1}{\sqrt{m^2+n^2}}\sin\left[\frac{2\pi m}{L}\left(x-\frac{L}{2}\right)\right]\cos\left(\frac{2\pi n}{L}y+\varphi_{i,j}\right), \tag{12}$$

where $\varphi_{i,j}$ is a random phase uniformly distributed on the circle.

TABLE I. Density of energy and enstrophy for the three considered cases.

| | Energy | Enstrophy |
|---|---|---|
| Smooth field | 0.64±0.01 | 0.8±0.05 |
| Forced field | 2.62±0.005 | 10.81±0.03 |
| Anisotropic field | 0.28±0.005 | 0.18±0.01 |

#### *2. Passive tracers*

It is important to take special care of the way the dynamics of the tracers are computed to characterize the possible anomalous properties of transport. If they exist, such anomalies should find their origin in the existence of "memory effects," namely, long time correlations, since the accessible range of velocities is finite. From this perspective, any source of randomness leading to memory loss due to the numerical scheme may then induce a spurious effective diffusive behavior. Moreover, the Hamiltonian nature of the tracer dynamics imposes necessarily the choice of a simplectic integrator.

We thus chose the sixth-order implicit Gauss-Legendre simplectic scheme to compute the trajectories [23], as this integration scheme was successfully used in systems of point vortices [8,9,24,25]. However, in order to avoid a possible source of noise, we had to compute the velocities of particles exactly, meaning that we performed an exact back-Fourier transform of the modes describing the evolution of the field. This constraint is numerically expensive, and explains our choice of a relatively low resolution of $128^2$ for the evolution of the field. In this setting, the evolution of passive tracers may be understood as describing the advection of particles in a flow field generated by $128^2$ modes interacting through Eq. (1).

### E. Field settings

As to the choice of parameters and initial conditions in Eq. (1), we considered three different cases, with quite different values for the parameters. As mentioned earlier, we chose as a starting base similar initial conditions, type of forcing, and size of the system, as in [3]. For the three considered cases, for given initial conditions, we let the system evolve until it becomes sufficiently stationary for the time span considered during simulation, $\tau_{final}=10^4$. Stationarity is considered as being reached by monitoring the evolution of the energy and enstrophy of the system (see Table I). When forcing is present (cases 2 and 3), the random phases of the forcing are updated all at once every $\delta\tau=2$. The values assigned to $A_0$ are, respectively, for the three cases 1.1, 0.001, 0.5. For the first case, as there was no forcing, we tried a decent amplitude; for the second case, with strong forcing, we let the forcing drive the system; and for the last case, we tried something intermediate. The motivation for these choices was to get three different stationary fields, as the focus of this paper is actually more the transport of test particles rather than the actual dynamics of the field.

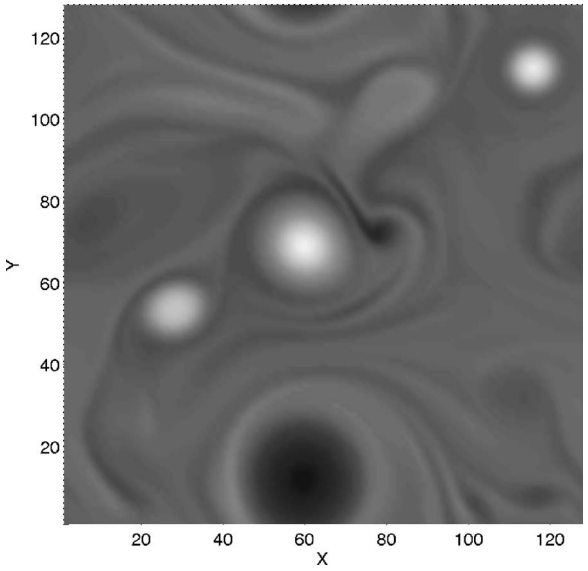


FIG. 1. Visualization of the field $-\Delta\Phi$ for the choice of parameters $\lambda=1$, $g=0.1$, $\nu=7\times10^{-6}$, $L=20$, and $N=128^2$ with no forcing. The field is "smooth" and appears as being isotropic. A few vortices are present. The gray coloring scheme scales from −4.5 (black) to 4.5 (white).

In order to visualize the field, we chose to use levels of the function $-\Delta\Phi$. The three considered cases are represented in Figs. 1–3.

#### *1. Smooth field*

To obtain the smooth field depicted in Fig. 1, we carried out simulations with no forcing ($F_0=0$) and a low dissipation. The parameters for this run were $\lambda=1$, $g=0.1$, $\nu=7\times10^{-6}$. Due to this low dissipation, the energy may be con-

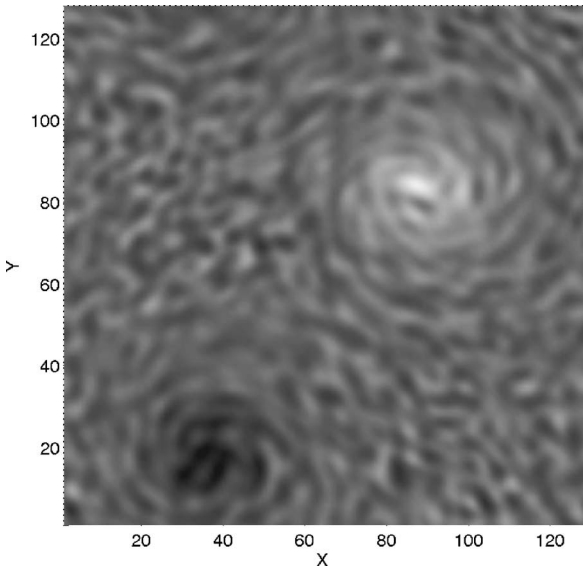


FIG. 2. Visualization of the field $-\Delta\Phi$ for the choice of parameters $\lambda=4$, $g=0.1$, $\nu=5\times10^{-5}$, $F_0=4$, $k_0=6\pm2$, and $\Delta t=2$. Two big perturbed vortices are present. The gray coloring scheme scales from −1.4 (black) to 1.4 (white).

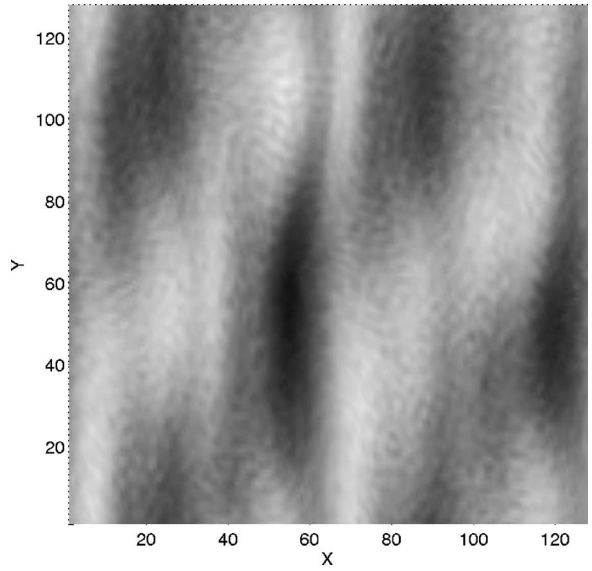


FIG. 3. Visualization of the field $-\Delta\Phi$ for the choice of parameters $\lambda=0.125$, $g=2$, $\nu=7.5\times10^{-6}$, $F_0=1.5$, $k_0=12\pm2$, and $\Delta t=2$. Elongated structures in the $y$ direction are present, marking a strong anisotropy. The gray coloring scheme scales from $-1.6$ (black) to 1.6 (white).

sidered as constant for the length of the simulation. We notice that a few distinct vortices are present. During the evolution, a merger between two vortices occurred. There is also an average drift in the $y$ direction.

#### *2. Forced field*

To obtain the forced field depicted in Fig. 2, we carried out simulations with a strong forcing and dissipation. The parameters for this run were $\lambda=4$, $g=0.1$, $\nu=5\times10^{-5}$, $F_0=4$, and $k_0=6\pm2$, and the phases for the random forcing were updated every $\Delta\tau=2$ time units. The value of $k_0$ corresponds to the physical scales of $\delta x\sim2\pi/k_0\approx1$. With this choice of parameters, the system consists of two perturbed vortices. An average drift in the $y$ direction is also noticeable.

#### *3. Anisotropic field*

To obtain the anisotropic field depicted in Fig. 3, we carried out simulations with some forcing and a high value for $g$. The parameters for this run were $\lambda=0.125$, $g=2$, $\nu=7.5\times10^{-6}$, $F_0=1.5$, and $k_0=12\pm2$. The value of $k_0$ corresponds to the physical scales of $\delta x\sim2\pi/k_0\approx0.5$. The phases for the random forcing are updated every $\Delta\tau=2$ time units. In this setting, elongated structures as well as a strong drift in the $y$ direction are present.

## III. TRANSPORT PROPERTIES

### A. Definitions

Unfortunately, the deterministic description of the motion of a passive particle in a chaotic region is impossible. Local instabilities produce exponential divergence of trajectories. Thus, even an idealized numerical experiment is nondeterministic, as round-off errors creep slowly but steadily from the smallest to the observable scale. The long-time behavior of tracer trajectories is then necessarily studied by using a probabilistic approach. In the absence of long-term correlations, the kinetic description, which uses the Fokker-Plank-Kolmogorov (FPK) equation, leads to Gaussian statistics. Yet, if a phenomenon with associated long-time correlations occurs, profound changes in the kinetics can be induced. These memory effects sometimes result in the modification of the diffusion coefficient in the FPK equation [26,27]. But often, their influence is more profound [7–9,28–30] and leads to non-Gaussian statistics and, for instance, to a nondiffusive behavior of the particle displacement variance

$$\langle(s-\langle s\rangle)^2\rangle\sim t^{\mu}, \tag{13}$$

where $\langle\cdots\rangle$ stands for ensemble averaging. Within this probabilistic approach, the main observables in order to characterize transport properties will be moments of the distributions

$$M_q(t)=\langle|s(t)-\langle s(t)\rangle|^q\rangle, \tag{14}$$

where $q$ denotes the moment order. The finiteness of velocity and of time in our simulations implies that all moments are finite and that a power law behavior is expected

$$M_q\sim D_q t^{\mu(q)}, \tag{15}$$

with, generally, $\mu(q)\neq q/2$, as would be expected for normal diffusion. The nonlinear dependence of $\mu(q)$ is a signature of the multifractality of the transport, while its linear dependence reflects a fractal situation [30–32]. In the fractal situation, all of the moments can be described by a single self-similar exponent $\nu$

$$\mu(q)=\nu\cdot q, \tag{16}$$

whereas the case when $\mu(q)$ is nonlinear

$$\nu(q)\equiv\frac{\mu(q)}{q}\neq\text{const}, \tag{17}$$

transport is multifractal. This distinction is important, since in the weak case, the PDF evolves in a self-similar way

$$P(s,t)=t^{-\nu}f(\xi),\quad \xi\equiv t^{-\nu}(s-\langle s\rangle), \tag{18}$$

while a nonconstant $\nu(q)$ in (17) precludes such self-similarity (see the discussions in [7,8] for details about non-self-similar behavior).

In order to characterize transport, we focus on the arc length $s(t)$ of the path traveled by an individual tracer up to a time $t$,

$$s_i(t)=\int_0^t v_i(t')dt', \tag{19}$$

where $v_i(t')$ is the absolute speed of the particle $i$ at time $t'$. This choice is motivated by the fact that in order to consider mixing properties from the dynamical principles, it is important to consider the trajectories within the phase space. However, for the system of passive particles, the phase space is formally "identical" to the physical space where particles evolve [see Eq. (9)]. Another important feature of the arc length is that it is independent of the coordinate system, and

as such, we can expect to infer intrinsic properties of the dynamics. Moreover, expression (19) implies that $s_i(t)$ reflects the history up to time $t$ of the speed $v_i$. Since the velocities are bounded, the observations described later on of anomalous transport behavior are directly linked to strong memory effects.

### B. Particle transport

We followed the evolution of 512 passive particles as defined by Eq. (8), and we computed $s_i(t)$'s up to a time $\tau = 10^4$. In order to keep a constant numerical accuracy, the increments $\Delta s_i(nT) = s_i[(n+1)T] - s_i(nT)$ were recorded for the successive diagnostic times $nT$. This last feature also has the advantage of providing better statistics when computing moments. Indeed, since we have chosen stationary regimes for the field, we can assume that transport properties are independent of the initial condition of the field and thus use time invariance to increase statistics. This time invariance becomes, however, not useful for times close to $\tau = 10^4$, and statistics in this region are thus not accurate anymore; also, we are not interested in short-time behavior. We have therefore considered times $10^2 < \tau < 5 \times 10^3$ in order to compute the $\mu(q)$.

In all three considered cases, the transport is found to be anomalous and superdiffusive, with a characteristic second-order exponent $\mu(2) \approx 1.8$ for all cases. The time behavior of the moments and characteristic exponents for all considered cases are plotted in Figs. 4–6, and a summary is provided in Table II, where we included for comparison the results obtained in Ref. [9] for a flow governed by point vortices. The similarity observed for the exponents in these quite different settings of the parameters and regimes of the Charney-Hasegawa-Mima equation, as well as the one observed in point vortices, points to a universal behavior for the transport of passive tracers in these two-dimensional flows, which in some sense confirms the validity of the quite general estimation of $\mu \approx 1.5$ proposed in [8] as a value for an universal exponent.

However, conversely to the point vortices case, one can see in Figs. 4–6 that the behavior of the characteristic exponent vs moment for the first two cases may correspond more to the multifractal type, although the nonlinearity is quite weak and error bars are quite large. In the third case, transport is more or less simply fractal. This behavior corresponds to simple fractal transport in the anisotropic system, which implies an almost self-similar behavior of the distribution function. In fact, as is illustrated in Fig. 5, we may expect that with more particles and larger times, the multifractal behavior may be more clear—a feature that can also be true for the third case. When computing characteristic exponents, one also has to recall the possibility of log-periodic oscillations [33]. This phenomenon may also be responsible for the uncertainties on the measured values of the exponents.

All in all, these results imply that at least for intermediate times, transport is anomalous and single fractal, which means that transport properties in these systems should be correctly described by a fractional Fokker-Plank-Kolmogorov equation of the type [6]

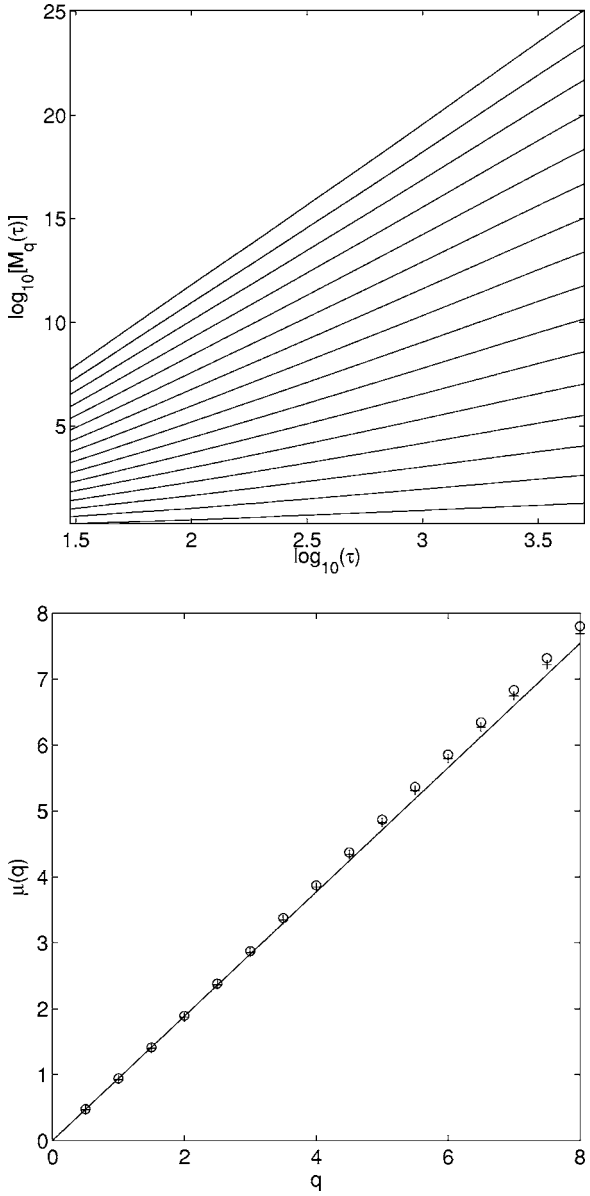


FIG. 4. Top: Moments of distribution of the arc length $M_q(\tau) = \langle |s(\tau) - \langle s(\tau) \rangle|^q \rangle$ vs time of tracers evolving in the smooth field for $q = 1/2, 1, 3/2, \ldots, 8$. The behavior $M_q(\tau) \sim \tau^{\mu(q)}$ is confirmed. Bottom: Characteristic exponent vs moment order, $q$ vs $\mu(q)$, with $\mu(2) = 1.87$. ○ and + symbols refer, respectively, to computations made using 512 and 256 particles. The solid line corresponds to $\mu(q) = \mu(1)q$, expected for self-similar behavior. Transport is superdiffusive and multifractal.

$$\frac{\partial^\beta P(s,t)}{\partial t^\beta} = \mathcal{D} \frac{\partial^\alpha P(s,t)}{\partial |s|^\alpha}, \tag{20}$$

with $\mu \approx 2\beta/\alpha$ (see for instance [6,8]). For larger times, transport may remain single fractal or develop a multifractal behavior, in which case, a model of transport properties using Eq. (20) may be only approximate. Note that using Eq. (20) to model transport properties implies that a kinetic limit has been performed on particle statistics. In this situation, we

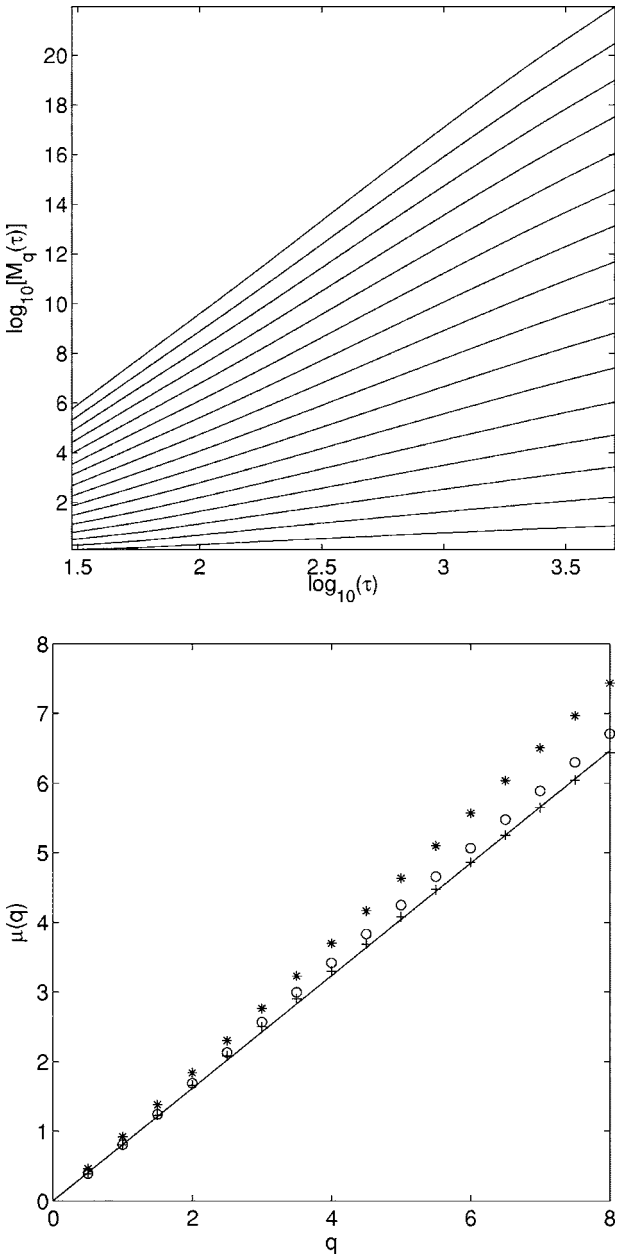


FIG. 5. Top: Moments of distribution of the arc length $M_q(\tau) = \langle |s(\tau) - \langle s(\tau) \rangle|^q \rangle$ vs time of tracers evolving in the forced field for $q = 1/2, 1, 3/2, \ldots, 8$. The behavior $M_q(\tau) \sim \tau^{\mu(q)}$ is confirmed. Bottom: Characteristic exponent vs moment order, $q$ vs $\mu(q)$, with $\mu(2) = 1.68$. Notice a change of slope after $\log_{10}(\tau_0) = 3.3$. The ○ and + symbols refer, respectively, to computations made using 512 and 256 particles for $\tau > \tau_0$, while the ∗ correspond to $\tau < \tau_0$. The solid line corresponds to $\mu(q) = \mu(1)q$, expected for self-similar behavior. Transport is superdiffusive.

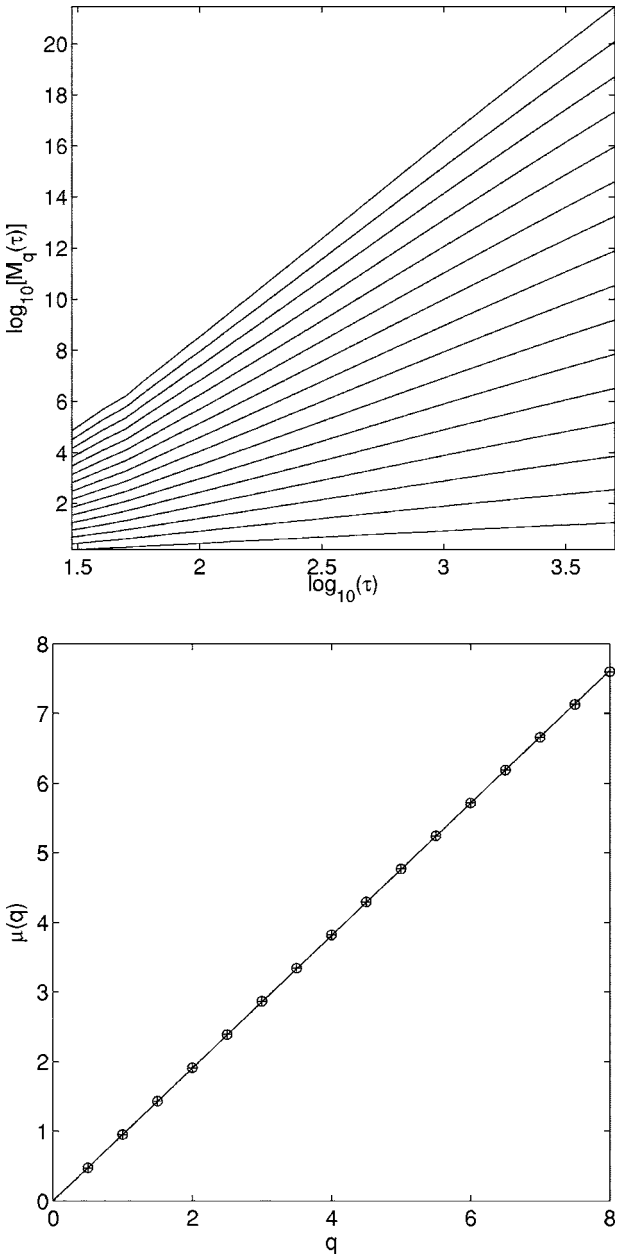


FIG. 6. Top: Moments of distribution of the arc length $M_q(\tau) = \langle |s(\tau) - \langle s(\tau) \rangle|^q \rangle$ vs time of tracers evolving in the anisotropic field for $q = 1/2, 1, 3/2, \ldots, 8$. The behavior $M_q(\tau) \sim \tau^{\mu(q)}$ is confirmed. Bottom: Characteristic exponent vs moment order, $q$ vs $\mu(q)$, with $\mu(2) = 1.85$. ○ and + symbols refer, respectively, to computations made using 512 and 256 particles. The solid line corresponds to $\mu(q) = \mu(1)q$, expected for self-similar behavior. Transport is super diffusive and single fractal.

are dealing with Levy-type processes, and hence, moments higher than two are likely not defined. This particularity is, however, linked to the kinetic limit, and since we are dealing numerically with a finite number of particles during a finite time, and also since velocities are bounded, moments of particle arc-length distribution are defined (see [34] for a discussion).

## IV. JETS

### A. Definitions

The origin of anomalous transport can be fairly well tracked when one is able to draw a phase portrait using a Poincaré map—for instance, to measure the Poincaré return time to a given region of phase space. This type of analysis will almost certainly lead to the conclusion that the phenomenon of stickiness on the boundaries of the islands generates

TABLE II. Characteristic second-moment exponent for the three cases studied. Exponents obtained in flows governed by point vortices in Ref. [9] are given for comparison.

| | |
|---|---|
| Point vortices | 4 vortices $\mu(2)\approx 1.82$ |
| | 16 vortices $\mu(2)\approx 1.77$ |
| Charney-Hasegawa-Mima | Smooth field $\mu(2)\approx 1.81$ |
| | Forced field $\mu(2)\approx 1.73$ |
| | Anisotropic field $\mu(2)\approx 1.85$ |

strong "memory effects," as a result of which transport becomes anomalous. However, when dealing with a more complex system, for which the drawing of a phase portrait is not achievable, one has to rely on other techniques.

In a two-dimensional phase space, the phenomenon of stickiness corresponds often to passive particles remaining for long times in the neighborhood of an island of regular motion. As a consequence of this behavior, sticky zones are regions where particles are trapped, and therefore are regions where particles remain in each other's neighborhood for long times. It then becomes natural, when dealing with more complex systems for which no phase portrait can easily be drawn, to look for places where passive particles remain in each other's vicinity for long times. One possible way to capture this feature of the dynamics is to look for its signature by measuring finite-time Lyapunov exponents (FTLEs), and by isolating within the space of initial conditions, regions of vanishing FTLEs (see for instance [35]). This type of approach, however, has its shortcomings, namely, sticky regions are not necessarily smooth from the microscopic point of view, meaning that they can be regions of strong chaos that are somehow restricted within an arbitrary small scale, which may be problematic when dealing with FTLEs. The other possibility is to look directly for chaotic jets [9]. These chaotic jets can be understood as moving clusters of particles within a specific domain for which the motion appears as almost regular from a coarse-grained perspective. From another point of view, looking for chaotic jets can be understood as a particular case of measurements of space-time complexity [12].

In order to look for jets, we proceed as illustrated in Fig. 7, which provides an easy and intuitive description of the mechanism used to detect jets. To summarize, we consider a reference trajectory $\mathbf{r}(t)$ within the phase space. We then associate with this trajectory a corresponding "coarse-grained" equivalent, i.e, the union of the balls $\cup B[\mathbf{r}(t),\epsilon]$ of radius $\epsilon$ whose center is the position $\mathbf{r}(t)$. Given an $\epsilon$ coarse-grained trajectory, we analyze the behavior of real trajectories starting from within the ball at a given time, and measure the time $\tau$ and length $s$, before the trajectory escapes from the coarse-grained trajectory. We then analyze the resulting distributions. This approach has already been used with success when studying numerically the advection of passive tracers in flows governed by point vortices [9]. The main difficulty in using this diagnostic follows from the fact that data acquisition is not sampled linearly in time or space, a point that leads in the present case to some difficulties.

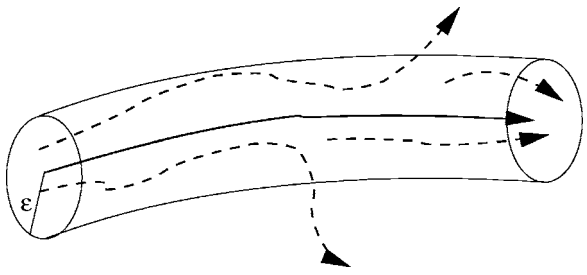


FIG. 7. Tracking of an $\epsilon$ coarse-grained regular jet.

### B. Statistical results

In the setting of the evolution of passive tracers within the three considered Charney-Hasegawa-Mima flows, we settled for the values $\epsilon=10^{-1}$ and $\delta=10^{-3}$. These values are to be compared with the values $\epsilon=10^{-2}$ and $\delta=10^{-6}$ considered for point vortex systems in [9]. This reduction of accessible scales stems from the fact that for the length of our simulations ($\tau=10^4$), only a few trajectories are escaping from the jets when we try to use the point vortex values. This leaves us with not enough data to gather realistic statistics. It is important to note that results should not depend much on the value of $\epsilon$ (see the discussion in [9]), as long as its value does not cross a characteristic scale in the system. For instance, in the point vortex systems, cores surrounding vortices had a radius of order $\sim 0.1$, and here in the forced systems, the characteristic wavelength corresponds to scales of order $\sim 1$. Moreover, in order to infer some possible fractal structure of the jet, we are constrained to consider the largest possible $\epsilon$ once $\delta$ has been fixed. Here, the choice made for $\delta$ was the smallest we could make in order to gather enough statistics, although these may not be sufficient for the anisotropic case. We also tried to keep at least two orders of magnitude between $\epsilon$ and $\delta$, to infer eventual fractal properties.

With the present choice of parameters, we were able to gather about 15 000 events for each of the three cases. We followed 256 reference trajectories for a time $\tau=10^4$ during which the behavior of two nearby tracers was checked. We defined as a reference trajectory the trajectory of a given passive tracer that evolves freely; we then positioned randomly at a distance $\delta$ from this tracer a second (or more) tracer, which was called a "ghost" in [9]. We then let these tracers evolve until the distance $\epsilon$ is reached. Then, the ghost is removed, and time interval $\Delta\tau$ and traveled length $\Delta s$ are recorded. A new ghost is assigned to the reference trajectory, and so on. We, of course, expect that the portion we compute of reference trajectory ($\tau=10^4$) is sufficiently ergodic in the accessible phase space.

We were then able to obtain the trapping-time distributions $\rho(\tau)$ described in Figs. 8–10. The characteristic exponent $\rho(\tau)\sim\tau^{-\gamma}$ for trapping times observed in two out of the three systems is typically $\gamma\approx 2.8$. For these cases, we therefore obtain good agreement with the relation

$$\gamma\approx\mu(2)+1, \tag{21}$$

which links the transport exponent $\mu$ to the characteristic trapping-time exponent. The law (21) can be linked to the

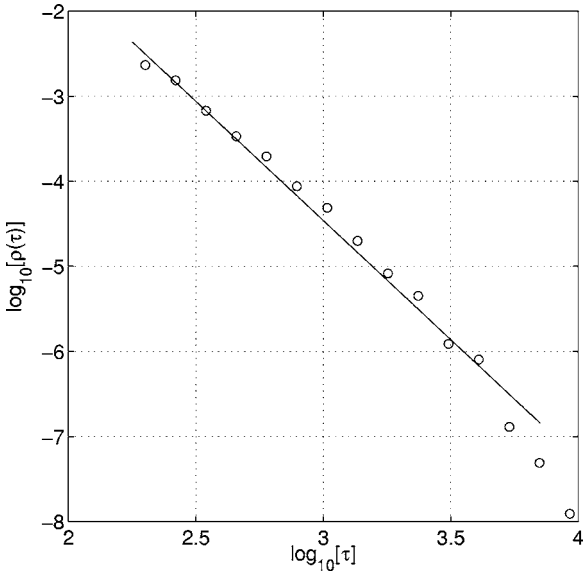


FIG. 8. Tail of the distribution of trapping times $\tau$ for the smooth field (see Fig. 1). A power-law decay is observed with typical exponent $\rho(\tau) \sim \tau^{-\gamma}$, with $\gamma \approx 2.8 \pm 0.1$.

fractional transport equation (20). One can link the $\gamma$ exponent to the $\beta$ exponent as follows: $\beta = \gamma - 1$, and $\mu = 2\beta/\alpha$ (see [8,9] and references therein). With $\alpha$ being linked to the spatial fractal properties, the Eq. (21) is valid when $\alpha \sim 2$. One can also see in Figs. 8 and 9 that the law $\rho(\tau) \sim \tau^{-\gamma}$ applies typically for times up to $\tau \sim 1000$ or a little more. This behavior can be expected, as we are following a finite number of reference trajectories (256) during a finite time ($\tau_{max} = 10^4$). In order to potentially obtain a broader range of applicability, one would have to increase the value of $\tau_{max}$ to at least $10^5$. This is unfortunately beyond our computing resources. Note also that due to the inverse cascade, there is an accumulation of energy at large scales, such that the driving

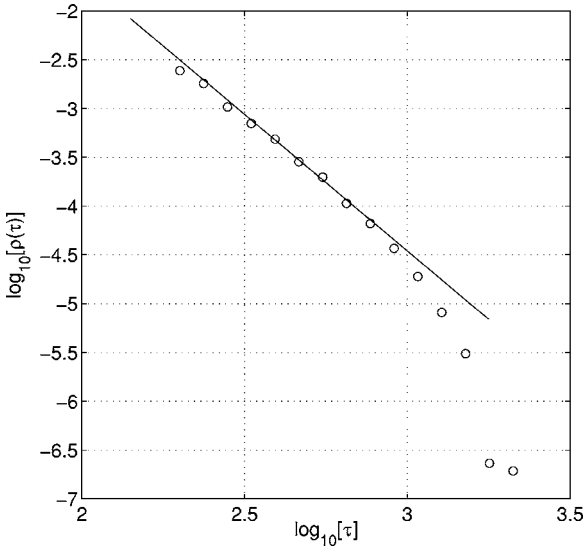


FIG. 9. Tail of the distribution of trapping times $\tau$ for the forced field (see Fig. 2). A power-law decay is observed with typical exponent $\rho(\tau) \sim \tau^{-\gamma}$, with $\gamma \approx 2.8 \pm 0.1$.

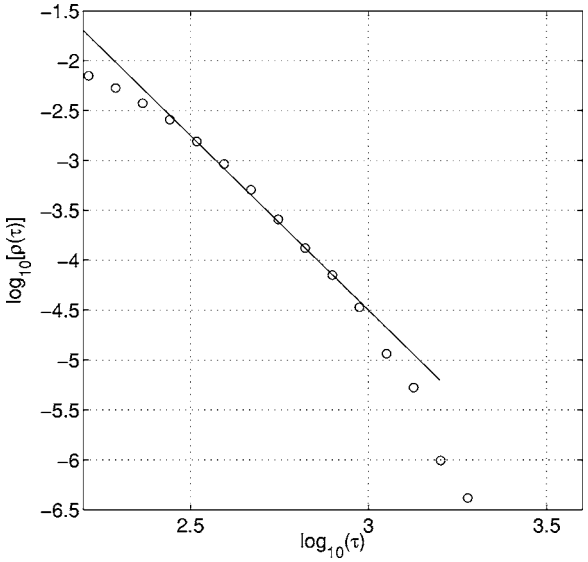


FIG. 10. Tail of the distribution of trapping times $\tau$ for the anisotropic field (see Fig. 3). A power-law decay is observed with typical exponent $\rho(\tau) \sim \tau^{-\gamma}$, with $\gamma \approx 3.5 \pm 0.5$.

field may not always be considered to have reached a stationary state if we decided to increase simulation length. In order get better statistics, one also has to be careful to not add too many particles instead of increasing time. Indeed, the limits $N \to \infty$ and $\tau \to \infty$ are most likely not commuting in these anomalous regimes where rare events related to memory effects are important.

In fact, the law (21) also applies in the anisotropic field for small trapping times, but over the whole range, it is clear (Fig. 10) that no scaling law really emerges. When compared with the two other cases, we may find two possible reasons for this failure. First, we can notice that in this configuration of the field, the energy and enstrophy are quite low, implying weak nonlinear effects. It may thus take more time to fill the tail of the trapping-time distribution. Second, another peculiarity of the anisotropic case is the fact [36,37] that in the anisotropic case, the conservation of the generalized vorticity $\Omega = \Phi - \lambda \Delta \Phi + gx$, by the evolution of the Hasegawa-Mima equation (1), implies necessarily that for strong values of $g$, the motion along the $x$ direction is bounded. Hence, in this situation, the motion of passive tracers is quasi-one-dimensional. In this setting, it is likely that the hidden fractal properties in the system may differ from those for a two-dimensional system, especially regarding the derivation of the laws linking $\beta$, $\gamma$, and $\alpha$. In this regard, the fact that the law (21) is valid for small times up to a time $\tau_c$ may just be a simple consequence of the fact that for $\tau < \tau_c$, the passive tracers have not yet reached the boundaries imposed by $g$, and a spatially two-dimensional behavior is still accurate. At this point, it is important to recall that we have periodic boundary conditions. The constraint imposed by the conservation of $\Omega$ is thus not as important for small values of $g$ corresponding to the first two cases.

The rarity of events with smaller values of $\delta$ indicates that the trajectories of tracers are relatively regular when one considers small scales, which implies the possibility of vanishing Lyapunov exponents. Hence, following the definitions given in [9]

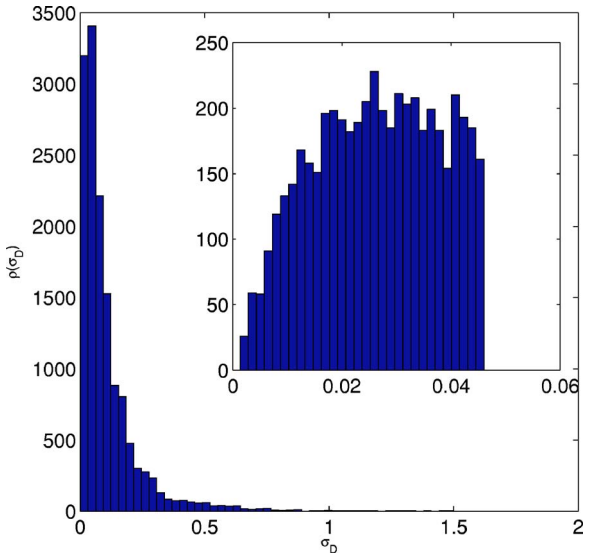


FIG. 11. (Color online) Unnormalized distribution of Lyapunov exponents $\sigma_D$ [see Eq. (23)]. An accumulation toward zero is observed. The inset, showing small regions, reveals an actual decrease for $\sigma_D < 0.02$; such behavior is expected, as data is bounded by finite speed and finite time.

$$\sigma_L = \frac{1}{\Delta t} \ln \frac{\epsilon}{\delta}, \tag{22}$$

$$\sigma_D = \frac{1}{\Delta s} \ln \frac{\epsilon}{\delta}, \tag{23}$$

we compute the distribution of Lyapunov exponents $\sigma_D$ obtained from the smooth-case data in Fig. 11, where one can directly see an accumulation toward zero of the distribution. The inset in Fig. 11 shows an actual decrease for $\sigma_D < 0.02$. This behavior is expected, as we have only finite speeds in the system and simulations are carried out for a finite time. For instance, $\sigma_D < 0.02$ corresponds to an average trapping time $t_a = 1100$. This accumulation of exponents toward zero is quite important, as it is strong evidence of memory effects. The system does not display universal hyperbolic properties, and thus transport modeling using this as a hypothesis are probably doomed. This also shows the relevance of the notion of weak chaos and weak mixing properties and, therefore, the necessity of considering simple models such as the billiard balls considered in [38]. Indeed, these results provide good insights on how the presence of quasi-zero Lyapunov exponents does not necessarily mean that the system is regular but that complexity is not growing as fast as expected [12].

### C. Localization and structure of jets

Due to the shape of the finite-size Lyapunov exponent distributions observed, it is also possible to track and localize the jets that are responsible for the anomalous behavior. Indeed, these exponents are monotonically decreasing. Hence, we can define a threshold beyond which the jet can be considered "regular." We can track the reference trajectory afterward in order to localize regions responsible for anomalous behavior. In Fig. 12, we show the localization of a jet for which the trapping time of nearby tracers is found to be $\approx 1000$ in the case of the forced field (see Fig. 2). The jet is bouncing back and forth between the two perturbed vortices. The procedure to detect a jet is quite simple—we choose a reference trajectory and then start to compute trapping times of ghosts. When we notice that a ghost has not escaped for a while (we choose $\tau > 200$ for this jet), we start recording the positions of the reference tracer. We also reset the ghosts and add many more in order to track the "structure" of the jet, and record their positions as well. When one of the ghosts leaves the jet, we measure the actual trapping time. If it appears long enough (here we chose $\tau > 1000$), we stop; otherwise, we reset everything and wait until the reference trajectories detect a new potential jet. The advantage of this method is that we have no *a priori* information about the jet location. For instance, the jet depicted in Fig. 12 was not anticipated, as we expected more a trapping within a vortex or in its neighborhood. We notice, however, that by using this method of detection, we miss the first portion of the jet. Note also that by localizing jets, we are able to detect regions responsible for the anomalous behavior of transport properties. It may, therefore, give a good clue about where and how to act on a system, if one wants to reduce or eliminate this anomaly.

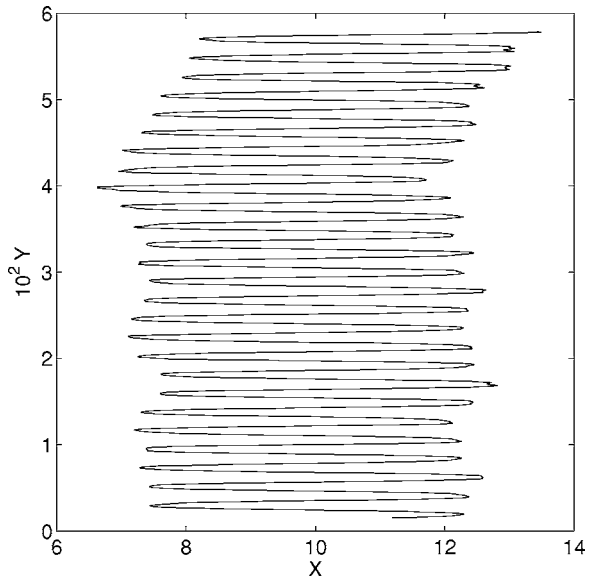


FIG. 12. Localization of a long-lived jet in the forced field (see Fig. 2). The jet is bouncing back and forth between the two perturbed vortices.

Once a jet is located, one can infer the behavior of the test tracers with respect to the reference trajectory. In order to create Fig. 13, 256 test particles were initialized on a circle around a reference particle whose trajectory was trapped in the long-lived jet localized in Fig. 12, and the relative positions of the test particles were plotted during the life of the jet. Notice the star like shape of the figure; this phenomenon is a consequence of multiple stretching and squeezing of the circle of particles, which one can observe while looking dynamically at the evolution of the circle. Notice also that

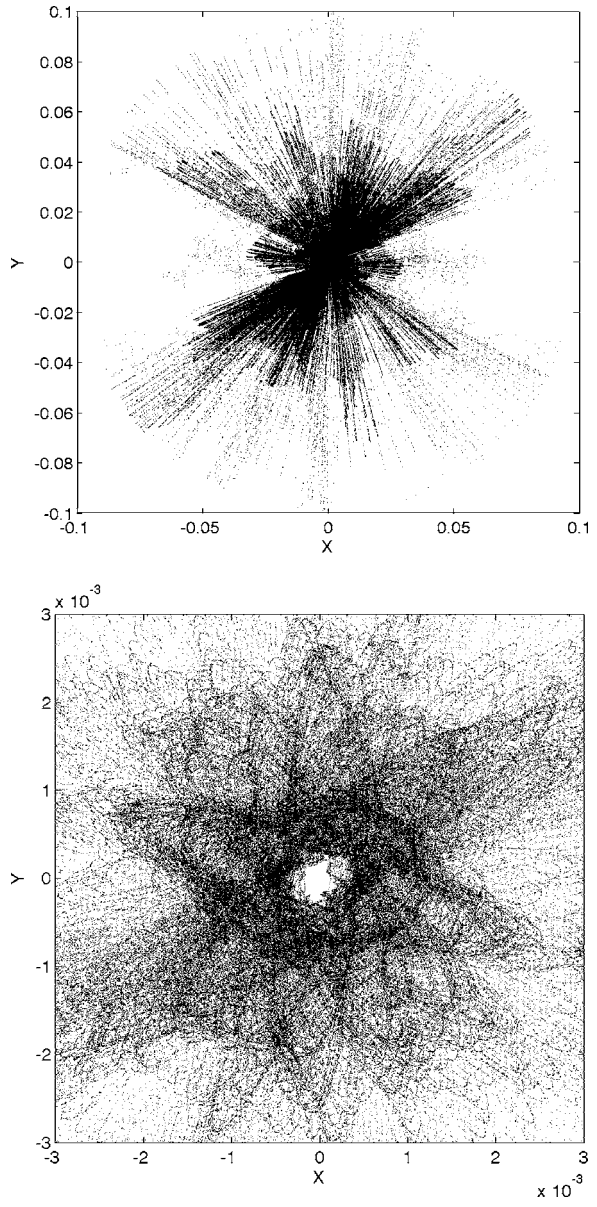


FIG. 13. (a) Relative position of test particles for the long-lived jet depicted in Fig. 12. (b) Test particles reach distances $<10^{-4}$ from the reference trajectory.

ghosts that initially are localized at a distance $\delta=10^{-3}$ from the reference tracer can find themselves much closer to the test particles close to $10^{-4}$ in Fig. 13. This implies that we do not expect that the value of the trapping-time exponent $\gamma$ is strongly dependent on the initial choice of $\delta$. Note also that the behavior portrayed in Fig. 13 seems to indicate that chaos is present at these scales; thus, contrary to our physical intuition, the relative motion within the jet is not regular. However, despite this fact, the chaotic behavior of trajectories is trapped within a given small scale for a long time, which in the end gives rise to a regular nondiffusive trajectory from a coarse-grained perspective. This trapping phenomena is also illustrated by the apparently "quantified" maximum radii seen on the star shape displayed in Fig. 13. We may thus speculate that these radii correspond to actual successive barriers that are restricting chaos within a small scale. Note also that the chaotic behavior within the jet may have induced numerical computations of strong values for finite-time Lyapunov exponents. In this situation, relying on these exponents would have meant that jets that are responsible for anomalous transport may go unnoticed.

## V. CONCLUSION

In this paper, we have investigated the dynamical and statistical properties of passive particle advection in different configurations of Charney-Hasegawa-Mima flows. The goal of this work was to consider transport properties of these systems while putting in perspective the results obtained for point vortex flows. In this sense, this provides qualitative insights on general transport properties of two-dimensional flows. The transport properties of all the considered cases are found to be anomalous with characteristic exponents $\mu \sim 1.75-1.8$. These values are also quantitatively comparable to the results obtained for point vortex flows.

In order to analyze the origin of the anomalous transport properties, passive tracer motion is analyzed by measuring the mutual relative evolution of two nearby tracers, i.e., by looking for chaotic jets [9]. The jets can be understood as moving clusters of particles within a specific domain, where the motion is almost regular from a coarse-grained perspective, inducing memory effects and long time correlations. The distribution of trapping times in the jets shows a power-law tail whose characteristic exponent is in very good agreement with the law $\gamma=\mu+1$ linking the transport exponent $\mu$ to the trapping-time exponent $\gamma$. This agreement is a good sign that the origin of anomalous transport in these system is intimately related to the existence of jets in the sense described earlier. The localization of jets in the system can be done, and it is shown that jets are not necessarily located around a coherent structure, as was the case for point vortex flows, but that they can manifest themselves by a trajectory bouncing back and forth between two structures. Moreover, when analyzing the structure of the jet, it is shown that the trajectory of individual tracers are likely chaotic within the jet, but that this chaotic behavior is for long times restricted within a given small scale, giving rise to the regular nondiffusive structure.

## ACKNOWLEDGMENTS

We would like to thank D. F. Escande for discussions, as well as corrections and suggestions regarding the manuscript. Part of the work presented in this paper was carried out while X.L. was visiting the Department of Fundamental Energy Science, Graduate School of Energy Science, Kyoto University; X.L. thanks S. Hamaguchi and A. Bierwage for useful discussions, as well as the department for financial support. G.M.Z. was supported by U.S. Navy Grant No. N00014-96-1-0055 and U.S. Department of Energy Grant No. DE-FG02-92ER54184.

[1] M. F. Schlesinger, G. M. Zaslavsky, and J. Klafter, Nature (London) **363**, 31 (1993).
[2] B. A. Carreras, V. E. Lynch, L. Garcia, M. Edelman, and G. M. Zaslavsky, Chaos **13**, 1175 (2003).
[3] S. V. Annibaldi, G. Manfredi, R. O. Dendy, and L. O'C. Drury, Plasma Phys. Controlled Fusion **42**, L13 (2000).
[4] D. del Castillo-Negrete, B. A. Carreras, and V. E. Lynch, Phys. Plasmas **11**, 3584 (2004).
[5] V. Grandgirard, O. Agullo, S. Benkadda, B. Biehler, X. Garbet, P. Ghendrih, and Y. Sarazin, in *Proceedings of the Varenna Conference*, 2000, edited by J. W. Connor, O. Sauter, and E. Sindoni, pp. 427–432.
[6] G. M. Zaslavsky, Phys. Rep. **371**, 641 (2002).
[7] L. Kuznetsov and G. M. Zaslavsky, Phys. Rev. E **61**, 3777 (2000).
[8] X. Leoncini, L. Kuznetsov, and G. M. Zaslavsky, Phys. Rev. E **63**, 036224 (2001).
[9] X. Leoncini and G. M. Zaslavsky, Phys. Rev. E **65**, 046216 (2002).
[10] V. V. Afanasiev, R. Z. Sagdeev, and G. M. Zaslavsky, Chaos **1**, 143 (1991).
[11] Xavier Leoncini and George M. Zaslavsky, Commun. Nonlinear Sci. Numer. Simul. **8**, 265 (2003).
[12] V. Afraimovich and G. M. Zaslavsky, Chaos **13**, 519 (2003).
[13] A. Hasegawa and A. Mima, Phys. Fluids **21**, 87 (1977).
[14] J. Pedlosky, *Geophysical Fluid Dynamics* (Springer-Verlag, New York, 1987).
[15] S. V. Annibaldi, G. Manfredi, and R. O. Dendy, Phys. Plasmas **9**, 791 (2002).
[16] V. Naulin, A. H. Nielsen, and J. Juul Rasmussen, Phys. Plasmas **6**, 4575 (1999).
[17] R. Dickman, Braz. J. Phys. **34**, 337 (2004).
[18] F. Dupont, R. I. McLachlan, and V. Zeitlin, Phys. Fluids **10**, 3185 (1998).
[19] J. Sukhatme, e-print physics/0410130 (unpublished).
[20] P. Beyer and S. Benkadda, Chaos **11**, 774 (2001).
[21] O. Agullo and A. Verga, Phys. Rev. E **69**, 056318 (2004).
[22] C. F. Fontán and A. Verga, Phys. Rev. E **52**, 6717 (1995).
[23] R. I. McLachlan and P. Atela, Nonlinearity **5**, 541 (1992).
[24] L. Kuznetsov and G. M. Zaslavsky, Phys. Rev. E **58**, 7330 (1998).
[25] A. Laforgia, X. Leoncini, L. Kuznetsov, and G. M. Zaslavsky, Eur. Phys. J. B **20**, 427 (2001).
[26] B. V. Chirikov, Phys. Rep. **52**, 263 (1979).
[27] A. B. Rechester and R. White, Phys. Rev. Lett. **44**, 1586 (1980).
[28] G. M. Zaslavsky, D. Stevens, and H. Weitzner, Phys. Rev. E **48**, 1683 (1993).
[29] D. del Castillo-Negrete, Phys. Fluids **10**, 576 (1998).
[30] P. Castiglione, A. Mazzino, P. Mutatore-Ginanneschi, and A. Vulpiani, Physica D **134**, 75 (1999).
[31] K. H. Andersen, P. Castiglione, A. Massino, and A. Vulpiani, Eur. Phys. J. B **18**, 447 (2000).
[32] R. Ferrari, A. J. Manfroi, and W. R. Young, Physica D **154**, 111 (2001).
[33] S. Benkadda, S. Kassibrakis, R. White, and G. M. Zaslavsky, Phys. Rev. E **59**, 3761 (1999).
[34] G. M. Zaslavsky, Physica A **288**, 431 (2000).
[35] S. Boatto and R. T. Pierrehumbert, J. Fluid Mech. **394**, 137 (1999).
[36] R. Basu, T. Jessen, V. Naulin, and J. J. Rasmussen, Phys. Plasmas **10**, 2696 (2003).
[37] R. Basu, V. Naulin, and J. J. Rasmussen, Commun. Nonlinear Sci. Numer. Simul. **8**, 477 (2003).
[38] G. M. Zaslavsky and M. Edelman, Chaos **11**, 295 (2001).